



## Room Temperature Electrically Injected Polariton Laser

Pallab Bhattacharya,<sup>†</sup> Thomas Frost, Saniya Deshpande, Md Zunaid Baten,  
Arnab Hazari, and Ayan Das<sup>\*</sup>

*Center for Photonics and Multiscale Nanomaterials, Department of Electrical Engineering and  
Computer Science, University of Michigan, 1301 Beal Avenue, Ann Arbor, Michigan 48109, USA*

(Received 25 November 2013; published 10 June 2014)

Room temperature electrically pumped inversionless polariton lasing is observed from a bulk GaN-based microcavity diode. The low nonlinear threshold for polariton lasing occurs at 169 A/cm<sup>2</sup> in the light-current characteristics, accompanied by a collapse of the emission linewidth and small blueshift of the emission peak. Measurement of angle-resolved luminescence, polariton condensation and occupation in momentum space, and output spatial coherence and polarization have also been made. A second threshold, due to conventional photon lasing, is observed at an injection of 44 kA/cm<sup>2</sup>.

DOI: 10.1103/PhysRevLett.112.236802

PACS numbers: 85.35.Be, 42.55.Sa, 71.36.+c, 78.45.+h

The possibility of generating coherent light by spontaneous radiative recombination from a coherent exciton-polariton condensate in a suitable microcavity was proposed by Imamoglu *et al.* [1]. Under conditions of strong coupling between cavity photons and excitons, new exciton-polariton eigenstates are created [2–6]. Polariton relaxation is made possible by polariton-phonon, polariton-electron, and polariton-polariton scattering. A coherent condensate at  $k \sim 0$  is produced by stimulated polariton-polariton scattering, which is a phase coherent process and which is the relevant gain mechanism. The separation of stimulation and emission leads to coherent emission without the requirement of population inversion. It is expected that the threshold energy for coherent emission from this device, called a “polariton laser,” would be much smaller than that of a conventional laser. Dynamic condensation of polaritons and polariton lasing in different material and nanostructure systems and with different dimensionality of the polaritons have been demonstrated in a series of elegant experiments using optical excitation [7–22], with a lowest reported threshold power of 120 nW [20], and a lowest threshold energy of 92 nJ/cm<sup>2</sup> [21]. Electrically pumped GaAs-based quantum well polariton lasers, operating at cryogenic temperatures, were recently demonstrated for the first time by Bhattacharya *et al.* [23] and Schneider *et al.* [24]. While this is a very important milestone in the development of this unique coherent light source, the realization of a room temperature electrically pumped device has remained elusive.

GaN-based room-temperature optically excited polariton lasers have been designed with all-semiconductor or hybrid dielectric-semiconductor microcavities having bulk, quantum well, or nanowire active regions [11,12,21,25,26]. Low-threshold operation of a bulk GaN electrically injected device has been theoretically predicted [27]. In this Letter we describe the room temperature operation of a bulk GaN diode microcavity in which current injection and optical feedback in the microcavity are in orthogonal directions.

The device operates as a polariton laser with an injection current threshold of 169 A/cm<sup>2</sup> (4 mA). The nonlinearity in the output characteristics is accompanied by linewidth narrowing and a small blueshift of the emission peak. We have measured and analyzed the polariton dispersion characteristics from which we derive a Rabi splitting of 32 meV. The measured population redistribution in momentum space and spatial coherence as a function of injection current confirm polariton condensation. The output polarization below and above threshold has also been characterized. Finally, a second threshold in the output corresponding to photon lasing by population inversion of injected carriers is observed at an injection level of 44 kA/cm<sup>2</sup> (1.04 A).

The bulk GaN diode consists of a 430 nm thick GaN *p-n* junction grown by plasma-assisted molecular beam epitaxy atop a 300 nm lattice matched *n*-doped In<sub>0.18</sub>Al<sub>0.82</sub>N layer on a GaN-on-sapphire substrate. The large band gap In<sub>0.18</sub>Al<sub>0.82</sub>N confines photons and minimizes substrate leakage of the electroluminescence. The microcavity itself consists of a 690 nm ( $5\lambda$ )  $\times$  40  $\mu$ m ridge defined by reactive ion etching and focused ion beam milling, with six and five pairs of SiO<sub>2</sub>/TiO<sub>2</sub> distributed Bragg reflector (DBR) mirrors deposited on opposite sides along the cavity length (690 nm). The fabrication and characteristics of the device are described in more detail in the Supplemental Material [28]. Polaritons in the microcavity are two dimensional. The device, which is schematically shown in Fig. 1(a), can also be viewed as an in-plane very short-cavity Fabry-Pérot laser. A plan-view scanning electron micrograph (SEM) of the device is shown in Fig. 1(b). Low excitation photoluminescence measurements (see Supplemental Material [28]) were made on undoped strain-free bulk GaN with light propagation perpendicular to the *c* axis. The  $X_A$  exciton transition is dominant up to room temperature and this has been considered in analysis of data [21,29–31]. The linewidth of this exciton transition at 10 K is 4.8 meV.

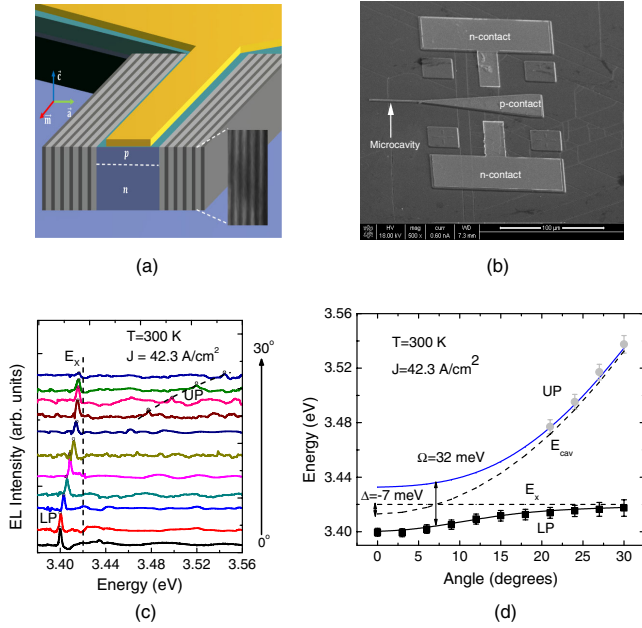


FIG. 1 (color online). (a) Schematic representation of the GaN microcavity diode. The inset shows a scanning electron microscopy image of the  $\text{SiO}_2/\text{TiO}_2$  DBR mirror on one side, (b) scanning electron microscopy image of the fabricated device, (c) angle resolved electroluminescence spectra measured at room temperature, (d) calculated polariton dispersion from a coupled harmonic oscillator model alongside the measured data of (c).

The quality factor ( $Q$ ) of the microcavity is derived to be 1911 from microphotoluminescence measurement (see Supplemental Material [28]) of the cavity mode at 3.413 eV with a linewidth  $\gamma_c = 1.7$  meV, corresponding to a cavity mode lifetime of 0.387 ps. Such a high value of  $Q$  is considered necessary to achieve low injection polariton lasing [32] and short-cavity photon lasing in this material system.

The polariton dispersion characteristics were determined from angle-resolved electroluminescence spectra measured under low forward bias current at room temperature and are shown in Fig. 1(c). The normal is along the length of the cavity and perpendicular to the DBR mirrors. Two distinctive features are observed in the spectra. A dominant peak is observed below the exciton ( $X_A$ ) resonance, which gradually approaches the exciton energy at large angles  $\sim 30^\circ$ . A much weaker peak is identified at energies above the exciton resonance at higher angles. The two peaks are identified as the lower (LP) and upper (UP) polariton transitions. No other transitions were visible in the spectra. The corresponding angle-resolved polariton dispersion characteristics are shown in Fig. 1(d). It should be noted that the identified UP transitions have energies that are resonant with continuum states within the band. Therefore there is some degree of uncertainty regarding their origin. The measured dispersions have been analyzed by the coupled oscillator model considering the strong coupling

of the cavity photon to the  $X_A$  exciton and are shown by the solid curves in Fig. 1(d) alongside the measured data. The cavity-to-exciton detuning  $\delta$  and the interaction potential, or Rabi splitting,  $\Omega$  are determined to be  $-7$  meV, and  $\sim 32$  meV, respectively. The splitting value is close to those reported for bulk GaN microcavities [33–35].

To investigate the nonlinear output characteristics of the GaN microcavity diode, the electroluminescence from the device was measured in the normal direction as a function of continuous wave (cw) forward bias. A distinct nonlinear threshold is observed in the light output at a current density of  $169$  A/cm $^2$  as shown in Fig. 2(a). This corresponds to a threshold current of 4 mA. However, it should be noted that the actual current through the microcavity region is much smaller. It may be noted from Fig. 2(a) that the slope of the light-current characteristics is sublinear in the prethreshold regime. We believe this behavior is due to nonradiative recombination and carrier leakage from the active recombination region and we have analyzed it with the relevant polariton rate equation in the steady state (see Supplemental Material [28]). The calculated output is shown alongside the measured data. The nonlinear threshold is accompanied by a steep reduction of the emission linewidth of the LP emission, also depicted in Fig. 2(a). The

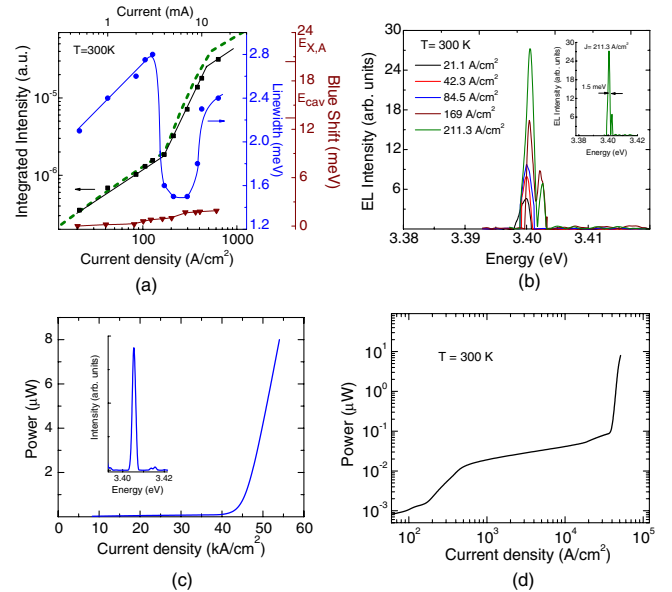


FIG. 2 (color online). Polariton and photon lasing characteristics at normal detection angle. (a) Integrated EL intensity, LP emission linewidth, and blueshift of peak emission as a function of injected current density. The solid lines are guides to the eye and the dashed green line shows the calculated intensities, (b) EL spectra measured at various injection levels. Inset shows the spectra above threshold (5 mA), (c) light-current characteristics of photon lasing observed in the same device at higher injection levels. Inset shows EL spectra measured above photon lasing threshold (1.04 A), (d) two threshold lasing behavior with the nonlinearities due to polariton and photon lasing.

LP spectral characteristics are shown in Fig. 2(b). Beyond  $380 \text{ A/cm}^2$ , the emission linewidth increases again due to exciton-exciton interaction. The LP density at the nonlinear threshold, taking into account all possible sources of uncertainties in the measurement, is calculated to be  $(4.7 \pm 1.1) \times 10^{16} \text{ cm}^{-3}$  with the relation  $n_{\text{LP}} = J\tau_{\text{total}}/qd$  where the measured total lifetime of excitons  $\sim 575 \text{ ps}$  (see Supplemental Material [28]) has been used. Also depicted in Fig. 2(a) is the measured small blueshift of the LP emission, caused by polariton-polariton and polariton-exciton interactions [36]. From the measured blueshift  $\delta E$  of  $1.9 \pm 0.28 \text{ meV}$  around the nonlinear threshold, the polariton density can be estimated using  $\delta E \cong 3.3\pi E_x^B a_B^3 N_{3D}$  [11]. Here  $E_x^B$  and  $a_B$  are the exciton binding energy and Bohr radius, respectively. Using values of  $E_x^B = (28 \pm 8) \text{ meV}$  [37,38] and  $a_B = (3.5 \pm 0.1) \text{ nm}$ , a value of  $N_{3D} = (1.53 \pm 1.13) \times 10^{17} \text{ cm}^{-3}$  is derived which is slightly larger than the value derived from the measured current density. A larger value results because the formula for the blueshift quoted above takes only phase space filling into account, while the measured blueshift can include both saturation of the oscillator strength and phase space filling. These densities are smaller than the transparency density of  $\sim 3 \times 10^{18} \text{ cm}^{-3}$  [39] and the Mott density of  $1\text{--}2 \times 10^{19} \text{ cm}^{-3}$  in GaN [11]. A value of the LP coherence time of  $\sim 2.8 \text{ ps}$  is calculated from the minimum linewidth of  $1.5 \text{ meV}$  in Fig. 2(a). With further increase of injection current and using a pulsed mode bias beyond  $2 \text{ kA/cm}^2$ , a second threshold is observed at  $44 \text{ kA/cm}^2$ . This second nonlinearity in the output, as shown in Fig. 2(c), is believed to be due to photon lasing via population inversion and stimulated emission. The linewidth of the emission for photon lasing is  $\sim 5 \text{ \AA}$  ( $4.6 \text{ meV}$ ), as shown in the inset to Fig. 2(c). Device heating lowers the energy of the peak by a small amount ( $1 \text{ nm}$  or  $12 \text{ meV}$ ). The two thresholds are shown together in Fig. 2(d). From the photon lasing threshold condition [40], we estimate the cavity loss to be  $\sim 31 \text{ cm}^{-1}$ . The novelty of the present device lies in the fact that a low resistance diode can be fabricated, strong feedback can be achieved with high quality DBR mirrors, and both polariton lasing and photon lasing can be observed.

The multimode nature of polariton lasing is evident in Fig. 2(b). Closely spaced peaks in polariton lasing spectra have been reported to be present in GaN [11], ZnO [18,19], and CdTe [8,41] microcavities. They ultimately result from strong localization of polariton modes. In our case, where 2–3 closely spaced peaks are observed [see inset of Fig. 2(b)], the average spacing is  $\sim 0.055 \text{ nm}$  ( $1.8 \text{ meV}$ ). The linewidths plotted in Fig. 2(a) are those of the dominant peak in the spectra. The GaN diode, grown on a GaN-on-sapphire template, has  $\sim 10^7\text{--}10^8 \text{ cm}^{-2}$  defects. We speculate that these defects can cause lateral filamentation along the width of the cavity, as in a broad-area photonic laser, and cause strongly localized polariton condensates. There can

also be small fluctuations in the optical thickness of the cavity along the width due to imperfections in the dielectric DBR. Both features will give rise to the spectrally separated modes.

The dynamic condensation of polaritons as a function of injection was also investigated. Figures 3(a)–3(c) show false color plots of the momentum distribution of polariton emission intensity obtained from angle resolved measurements for different injection currents. Below the threshold current density, the emission exhibits a broad distribution in both energy and momentum, whereas above threshold for  $J = 422.5 \text{ A/cm}^2$ , a condensate is formed around  $k_{\parallel} \sim 0$  with  $\Delta E = 1.3 \text{ meV}$  and  $\Delta k = 0.53 \times 10^4 \text{ cm}^{-1}$  (the angular resolution of measurement corresponds to  $\Delta k \sim 0.30 \times 10^4 \text{ cm}^{-1}$ ). The multimode polariton emission discussed above is evident in the false color plots. The LP occupancy in  $k_{\parallel}$  space for different injection levels is plotted in Fig. 3(d). From a nonthermal distribution below threshold, a Boltzmann-like distribution emerges just below and at threshold. A bimodal distribution and strong peaking of the occupation at and near  $k_{\parallel} = 0$  is observed for injection above threshold. From a fit to the data for  $I = 2.5I_{\text{th}}$  a value of the normalized chemical potential,  $\alpha = -\mu/k_B T_{\text{LP}} = \ln(1 + N_0^{-1}) = 0.059$  is derived, confirming the establishment of quantum degeneracy in the system. There is no evidence of a polariton relaxation bottleneck at any injection level.

The condensation of the polaritons was further investigated by measuring the spatial polariton distribution with

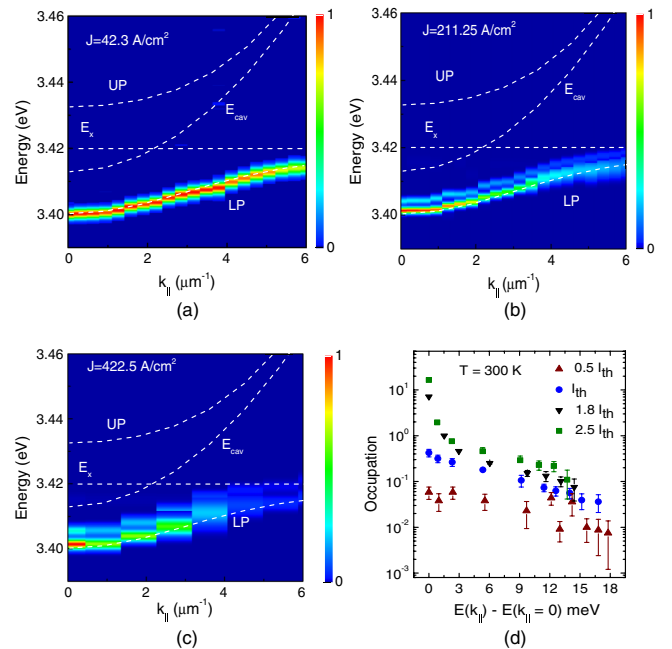


FIG. 3 (color online). (a)–(c) False color plots of energy-momentum distribution of polaritons at different current injection densities obtained from angle resolved EL measurements. (d) LP ground state occupancy for different  $k_{\parallel}$  states obtained from angle-resolved data.

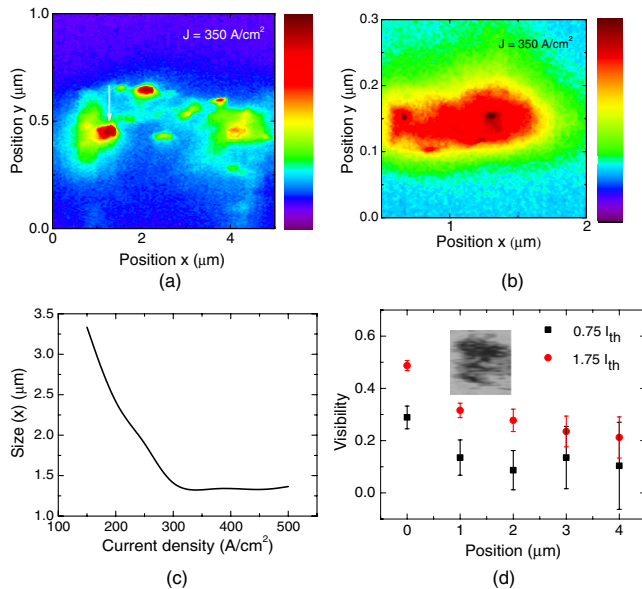


FIG. 4 (color online). Spatial distribution and coherence of polariton condensates above threshold showing (a) multiple condensate droplets, (b) enlarged image (by 3.3 times) of a single condensate identified by the arrow, (c) variation of condensate size with injection level, and (d) interference visibility measured as a function of the displacement between a double image of the polariton emission below and above threshold current. Inset shows interference pattern for  $x = 1 \mu\text{m}$ .

near field imaging and its coherence. Below threshold the uniform incoherent emission is observed (see Supplemental Material [28]), which transforms to multiple condensates as threshold is approached. These are coexisting nonequilibrium polariton condensates that are formed as a result of defects in the active region and are shown in Figs. 4(a) and 4(b). The width of the indicated island is plotted in Fig. 4(c) as a function of injection current. It is quite likely that the spectrally separated peaks in the polariton lasing spectra may originate from the different spatially isolated condensates. It is known that polariton lasing generally originates from a nonequilibrium Bose-Einstein condensate (BEC) obtained by a dynamical balance between injection and polariton (photon) loss. One of the characteristics of this condensate, similar to that of an equilibrium BEC, is long-range spatial coherence. We have measured the spatial coherence properties of the polariton emission with a Mach Zehnder interferometer [23]. The visibility of the observed fringes is plotted in Fig. 4(d) as a function of displacement ( $x$ ) between the two identical images of polariton emission. A value of  $\sim 48\%$  is obtained for  $I = 1.75I_{\text{th}}$ . While peak visibility should ideally approach unity at  $x = 0$ , such high values have not been experimentally reported. Several potential reasons have been cited, including quantum fluctuations in the condensate and the theoretical prediction that the condensate fraction of the polariton gas should be less than 50% [42]. The full width at half maximum (FWHM) of

the distribution gives an estimate of the spatial coherent length or size of the condensate. In this case, a condensate of  $\sim 1.5 \mu\text{m}$  is estimated, which is in good agreement with the data of Figs. 4(b) and 4(c). We have also measured the polarization of the  $k_{\parallel} \sim 0$  polariton emission as a function of injection. The emission is depolarized at low current injection levels. Above threshold a linear polarization of 30% develops spontaneously.

In conclusion, we demonstrate polariton lasing from a bulk GaN microcavity diode at room temperature. The nonlinear threshold is observed at  $169 \text{ A/cm}^2$ . Conventional photon lasing is also measured in the same device at a higher injection current density. The coherent output observed from a polariton device is due to a physical process that is very different from stimulated emission of radiation in a conventional photon laser. The device reported here has a threshold current density almost a hundred times smaller than GaN-based edge-emitting and surface-emitting lasers [43–46]. This first demonstration of room temperature operation of such a device with electrical injection opens up the possibility of realizing useful ultra-low energy coherent light sources with a variety of materials and should help to move the field of light-matter coupling into a more applied arena.

This work is supported by the National Science Foundation under the MRSEC program (Grant No. DMR-1120923) and by Grant No. ECS 1220715. The authors thank Bo Xiao for the help provided by him. One of us (T. F.) acknowledges the support provided by a National Science Foundation Graduate Research Fellowship.

\*ayan.das@intel.com

Present address: Intel Corporation, Hillsboro, Oregon 97124, USA.

†pkb@eecs.umich.edu

- [1] A. Imamoglu, R. J. Ram, S. Pau, and Y. Yamamoto, *Phys. Rev. A* **53**, 4250 (1996).
- [2] C. Weisbuch, M. Nishioka, A. Ishikawa, and Y. Arakawa, *Phys. Rev. Lett.* **69**, 3314 (1992).
- [3] G. Khitrova, H. M. Gibbs, F. Jahnke, M. Kira, and S. W. Koch, *Rev. Mod. Phys.* **71**, 1591 (1999).
- [4] H. Deng, G. Weihs, D. Snoke, J. Bloch, and Y. Yamamoto, *Proc. Natl. Acad. Sci. U.S.A.* **100**, 15318 (2003).
- [5] D. Porras, C. Ciuti, J. J. Baumberg, and C. Tejedor, *Phys. Rev. B* **66**, 085304 (2002).
- [6] L. V. Butov, C. W. Lai, A. L. Ivanov, A. C. Gossard, and D. S. Chemla, *Nature (London)* **417**, 47 (2002).
- [7] R. Huang, Y. Yamamoto, R. André, J. Bleuse, M. Muller, and H. Ulmer-Tuffigo, *Phys. Rev. B* **65**, 165314 (2002).
- [8] M. Richard, J. Kasprzak, R. Romestain, R. André, and L. S. Dang, *Phys. Rev. Lett.* **94**, 187401 (2005).
- [9] H. Deng, D. Press, S. Götzinger, G. S. Solomon, R. Hey, K. H. Ploog, and Y. Yamamoto, *Phys. Rev. Lett.* **97**, 146402 (2006).
- [10] J. Kasprzak *et al.*, *Nature (London)* **443**, 409 (2006).
- [11] S. Christopoulos *et al.*, *Phys. Rev. Lett.* **98**, 126405 (2007).

- [12] G. Christmann, R. Butté, E. Feltin, J. Carlin, and N. Grandjean, *Appl. Phys. Lett.* **93**, 051102 (2008).
- [13] D. Bajoni, P. Senellart, E. Wertz, I. Sagnes, A. Miard, A. Lemaître, and J. Bloch, *Phys. Rev. Lett.* **100**, 047401 (2008).
- [14] D. Bajoni, E. Semenova, A. Lemaître, S. Bouchoule, E. Wertz, P. Senellart, and J. Bloch *et al.*, *Phys. Rev. B* **77**, 113303 (2008).
- [15] S.I. Tsintzos, N.T. Pelekanos, G. Konstantinidis, Z. Hatzopoulos, and P.G. Savvidis, *Nature (London)* **453**, 372 (2008).
- [16] M. Nomura, N. Kumagai, S. Iwamoto, Y. Ota, and Y. Arakawa, *Nat. Phys.* **6**, 279 (2010).
- [17] S. Kéna-Cohen and S.R. Forrest, *Nat. Photonics* **4**, 371 (2010).
- [18] T. Guillet *et al.*, *Appl. Phys. Lett.* **99**, 161104 (2011).
- [19] Feng Li *et al.*, *Appl. Phys. Lett.* **102**, 191118 (2013).
- [20] S. Azzini, D. Gerace, M. Galli, I. Sagnes, R. Braive, A. Lemaître, J. Bloch, and D. Bajoni, *Appl. Phys. Lett.* **99**, 111106 (2011).
- [21] A. Das, J. Heo, M. Jankowski, W. Guo, L. Zhang, H. Deng, and P. Bhattacharya, *Phys. Rev. Lett.* **107**, 066405 (2011).
- [22] S. Brodbeck *et al.*, *Opt. Express* **21**, 31098 (2013).
- [23] P. Bhattacharya, B. Xiao, A. Das, S. Bhowmick, and J. Heo, *Phys. Rev. Lett.* **110**, 206403 (2013).
- [24] C. Schneider *et al.*, *Nature (London)* **497**, 348 (2013).
- [25] J. Heo, S. Jahangir, B. Xiao, and P. Bhattacharya, *Nano Lett.* **13** (6), 2376 (2013).
- [26] K. Daskalakis *et al.*, *Appl. Phys. Lett.* **102**, 101113 (2013).
- [27] D. Solnyshkov, E. Petrolati, A. Di Carlo, and G. Malpuech, *Appl. Phys. Lett.* **94**, 011110 (2009).
- [28] See Supplemental Material for a description <http://link.aps.org/supplemental/10.1103/PhysRevLett.112.236802> of the device structure and characteristics, and the optical characteristics.
- [29] R. Butté, G. Christmann, E. Feltin, J.F. Carlin, M. Mosca, M. Ilegems, and N. Grandjean, *Phys. Rev. B* **73**, 033315, (2006).
- [30] A. Das, P. Bhattacharya, J. Heo, A. Banerjee, and W. Guo, *Proc. Natl. Acad. Sci. U.S.A.* **110**, 2735 (2013).
- [31] A. Teke and H. Morkoç, in *Springer Handbook of Electronic and Photonic Materials*, edited by S. Kasap and P. Capper (Springer, New York, 2007), p. 778.
- [32] D. Solnyshkov and G. Malpuech, *Superlattices Microstruct.* **41**, 279 (2007).
- [33] M. Gurioli, M. Zamfirescu, F. Stokker-Cheregi, A. Vinattieri, I.R. Sellers, F. Semond, M. Leroux, and J. Massies, *Superlattices Microstruct.* **41**, 284 (2007).
- [34] I.R. Sellers *et al.*, *Phys. Rev. B* **74**, 193308 (2006).
- [35] F. Stokker-Cheregi *et al.*, *Appl. Phys. Lett.* **92**, 042119 (2008).
- [36] N. Peyghambarian, H. M. Gibbs, J.L. Jewell, A. Antonetti, A. Migus, D. Hulin, and A. Mysyrowicz, *Phys. Rev. Lett.* **53**, 2433 (1984).
- [37] I. Vurgaftman and J.R. Meyer, *J. Appl. Phys.* **94**, 3675 (2003).
- [38] G. Christmann, R. Butté, E. Feltin, A. Mouti, P.A. Stadelmann, A. Castiglia, J.-F. Carlin, and N. Grandjean, *Phys. Rev. B* **77**, 085310 (2008).
- [39] W. Fang and S.L. Chuang, *Appl. Phys. Lett.* **67**, 751 (1995).
- [40] G. Cosendey, A. Castiglia, G. Rossbach, J. Carlin, and N. Grandjean, *Appl. Phys. Lett.* **101**, 151113 (2012).
- [41] M. Richard, J. Kasprzak, R. André, R. Romestain, L. S. Dang, G. Malpuech, and A. Kavokin, *Phys. Rev. B* **72**, 201301(R) (2005).
- [42] D. Sarchi and V. Savona, *Phys. Rev. B* **75**, 115326 (2007).
- [43] K. Omae, Y. Higuchi, K. Nakagawa, H. Matsumura, and T. Mukai, *Appl. Phys. Express* **2**, 052101 (2009).
- [44] C. Skierbiszewski *et al.*, *Appl. Phys. Lett.* **86**, 011114 (2005).
- [45] M. Zhang, A. Banerjee, C.-S. Lee, J.M. Hinckley, and P. Bhattacharya, *Appl. Phys. Lett.* **98**, 221104 (2011).
- [46] T. Frost, A. Banerjee, K. Sun, S.L. Chuang, and P. Bhattacharya, *IEEE J. Quantum Electron.* **49**, 923 (2013).